photonics

MDPI

Article

Array-Patterned Micro-Structures in Spectacle Lenses Designed for Myopia Control via Image Blur †

Huilv Jiang, Zengwei Zhao, Quan Yuan, Yiqian Li, Ke Ma, Yaoyao Fu, Jiaojie Chen, Jun Jiang and Yiyu Li *

National Engineering Research Center of Ophthalmology and Optometry, Eye Hospital, Wenzhou Medical University, Wenzhou, 325027, China; jianghuilv@wmu.edu.cn (H.J.); zengweizhao55@163.com (Z.Z.); yuanquan202303@163.com (Q.Y.); 13587869379@163.com (Y.L.); kema0129@163.com (K.M.); fuyaoyao_1217@wmu.edu.cn (Y.F.); chenjiaojie@wmu.edu.cn (J.C.); jiangjwz@wmu.edu.cn (J.J.)

* Correspondence: liyiyu@wmu.edu.cn

† This article is a revised version of a paper entitled "Array-patterned micro-structures in spectacle lens for myopia control via image blurry", which was presented at SPIE Photonics Asia 2024, Nantong, China, 12–14 October 2024.

Abstract: Using micro-structure components in spectacle lenses has enabled myopia progression control in children and teenagers. However, the optical design of these spectacle lenses has never been discussed, leading to a lack of correct understanding of the underlying optical treatment principles. In this work, array-patterned hexagonal lenslets with two powers of opposite signs were proposed to construct a lenslet array-integrated (LARI) spectacle lens developed for an ongoing, randomized, controlled clinical trial and to support the optical approach to myopia control leveraging retinal image blur. We found that the phase modulation induced by the micro-structures of the lenslet array contributes to the increase in RMS wavefront aberrations, leading to image blur, further inspiring the novel array-patterned micro-structure design with high-order phase elements (HOPEs). The optical performance of both LARI and HOPE spectacle lenses was investigated by simulation and experiment.

Keywords: lenslet array; phase modulation; myopia control; spectacle lens

Received: 4 November 2024
Revised: 23 January 2025
Accepted: 24 January 2025
Published: 26 January 2025

Citation: Jiang, H.; Zhao, Z.; Yuan, Q.; Li, Y.; Ma, K.; Fu, Y.; Chen, J.; Jiang, J.; Li, Y. Array-Patterned Micro-Structures in Spectacle Lenses Designed for Myopia Control via Image Blur. *Photonics* **2025**, *12*, 110. https://doi.org/10.3390/photonics12020110

1. Introduction

Optical interventions including overnight orthokeratology [1,2], spectacle lenses [3], and soft contact lenses [4–6] were developed to slow the progression of myopia. The working principle of these optical interventions is usually believed to be based on the presence of relatively myopic peripheral defocus on the retina [7–9]. However, the basic hypothesis that a relatively hyperopic peripheral defocus can potentially also help control human myopia remains unproven [10,11]. Recently, several randomized controlled clinical trials (RCTs) [12–14] have reported success in controlling myopia progression with novel spectacle lenses featuring the array-patterned micro-lenses or micro-cylinders arranged on the surrounding lens surface. The positive powers of these micro-structures locally applied to the base optic lenses are very likely to be mistaken for being associated with the effect of relatively myopic peripheral defocus. Luckily, a series of further investigations [15–19] about the optical performance of these spectacle lenses suggested that there may be a new pathway between image blur or the decrease in image contrast and the myopia progression control, which might play a role in slowing myopia progression by using spectacle lens with lenslets. Until now, the treatment principle of these optical interventions remained uncertain. Therefore, it is necessary to design a new type of spectacle lens with lenslets for myopia control to support these theories.

A two-year RCT currently implemented at the Eye Hospital of Wenzhou Medical University (WMU) is expected to clarify the optical treatment principle [20]. To support the RCT, we designed a new spectacle lens embedded with array-patterned hexagonal lenslets and named it a lenslet array-integrated (LARI) spectacle lens. This double-masked RCT started in 2022. The subjects were randomly allocated to wear LARI spectacle lenses with positive lenslets (PLARI, treatment group one), LARI spectacle lenses with negative lenslets (NLARI, treatment group two), or single-vision spectacle lenses (control group). The aim of the present manuscript, which is based on a previous conference report [21], is to prove the same imaging performance between the two kinds of LARI spectacle lenses. In so doing, the expected similar myopia control efficacy of both treatment groups will be not enough to explain with the relatively myopic peripheral defocus but will presumably be explained with image blur. In this process, we will address the issues regarding the design, simulation, and manufacture of these LARI spectacle lenses. Furthermore, inspired by the causal link between image blur and the RMS wavefront aberrations caused by the phase modulation of the lenslet array in the LARI case, we will propose a series of novel designs of array-patterned micro-structures with high-order phase elements (HOPEs) in spectacle lenses for myopia control applications.

2. Design of LARI Spectacle Lens

The spectacle lens employs spherical base surfaces. The micro-structures are distributed on the region surrounding the clear center of the front lens surface and composed of hexagonal lenslets arranged tightly in a hexagonal pattern, as shown in Figure 1a. Each lenslet that is neighbored by six adjacent lenslets continues the base surface power and is represented by a blank, so the fill factor of the lenslets in the micro-structure region is estimated to be 66.7%. In the area of the blanks, the spherical base surface plays an optical role. The micro-structures are absent in the central optical zone of the lens, which has an aperture of about 8 mm in diameter and is reserved for providing the measurement of lens refractive power and the refractive correction for distance vision. Two different LARI spectacle lenses were designed with the lenslet of +3.00 D addition power (PLARI) and −3.00 D addition power (NLARI), respectively, as shown in Figure 1. The lenslets are arranged at a constant grid pitch of 1.2 mm. The maximum sag offset of the lenslets relative to the base surface, which has a radius curvature of 253 mm, is calculated to be about 1.2 μm. The refractive index used for the lens material is 1.586.

The spherical base surface in the central optical zone of the spectacle lens focuses rays from distant objects on the retina (image plane), as shown in Figure 2. The lenslets with +3.00 D addition power in the micro-structure region focus rays in front of the retina, and the lenslets with −3.00 D addition power in the micro-structure region focus rays behind the retina. However, different lenslets form multiple separate focal points, and all the wavefronts formed on the same retinal area, are superimposed to form a new wavefront, resulting in low-order wavefront aberration. This technology is protected by Patent Cooperation Treaty (WO2023/065556A1).

The optical performance of the LARI spectacle lens was simulated in a lens–eye system by the three-dimensional ray tracing method in custom MATLAB software (R2023a, MathWorks). In the simulation system, the origin of the coordinate is set at the vertex of the anterior lens surface. The posterior and front lens surfaces have radius curvatures of 176.5 mm and 253 mm to give the lens power of −1.00 D. The central thickness is set to be 1.5 mm. The distance from the vertex of the posterior lens surface to the rotation center of the eye is set to be 24 mm. The simulation was performed for four gaze directions represented by their chief rays starting from the rotation center of the eye. The four gaze directions were determined by the selected positions of the chief rays on the lens surface,

whose coordinates are (4, 4), (6, 6), (8, 8), and (10, 10); thus, the gaze angles were 13.3°, 19.5°, 25.2°, and 30.5°, respectively. The intersection points of the chief rays and the lens surface are evenly arranged by a fixed spacing and marked as the red circles shown in Figure 3a.

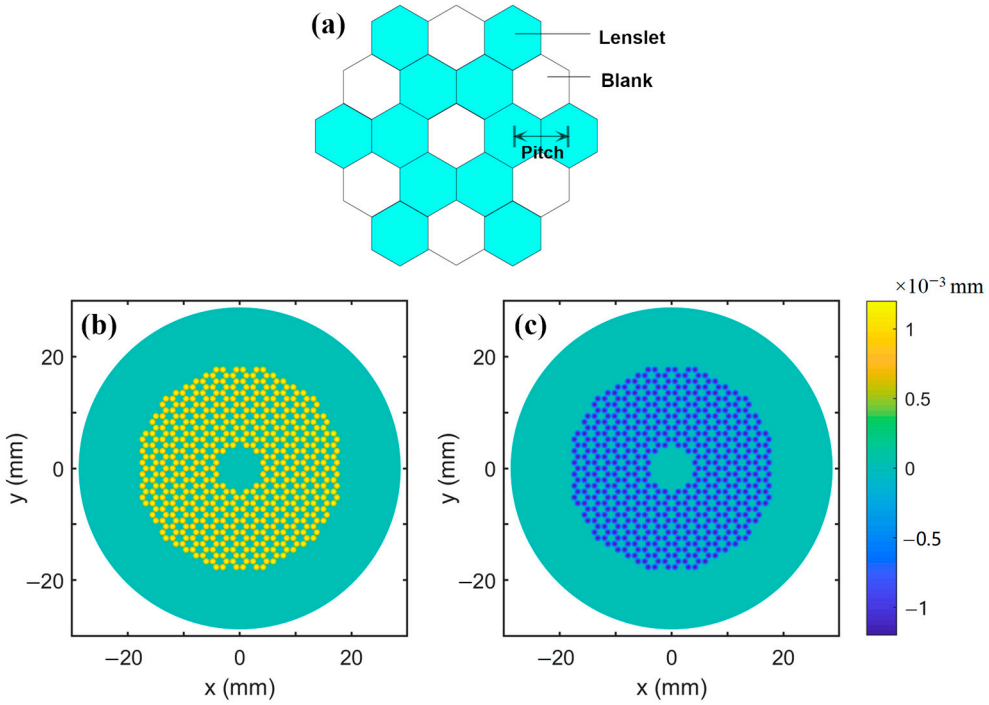

Figure 1. The micro-structure design of a lenslet array-integrated (LARI) spectacle lens. The radius curvature of the spherical base surface of the lens is 253 mm. The micro-structures are constructed by (**a**) the hexagonal arrangement of the lenslets. The blanks represent the distribution of the lenslets that continue the base surface power. The sag profile of micro-structures of (**b**) positive LARI (PLARI) or (**c**) negative LARI (NLARI) is on the micrometer scale using the base sphere as the reference surface.

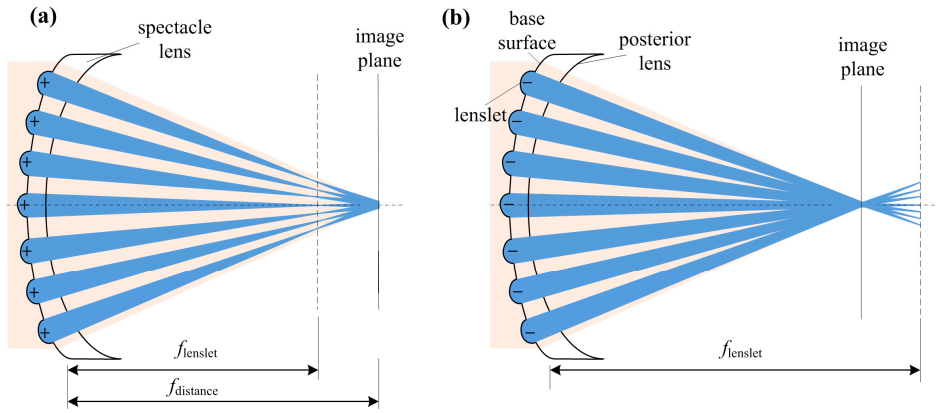

Figure 2. Schematic ray tracing of LARI spectacle lens with lenslets of +3.00 D addition power (**a**) and −3.00 D addition power (**b**), and lenslets form multiple separate focal point (lenslet with plus power focuses in front of distance focal plane and lenslet with minus power focuses behind distance focal plane). $f_{lenslet}$: focal length of lenslets, $f_{distance}$: focal length of spherical base surface.

For each gaze direction, a large number of rays were traced from the object point located at infinity to go through the lens, as shown in Figure 3b, and terminate at the vertex sphere whose center coincides with the rotation center of the eye. The calculated rays filled in an aperture of 8 mm in diameter to cover the general size of the pupil. The ray tracing calculation was based on the numerical algorithms programmed in Matlab codes, as previously described [22].

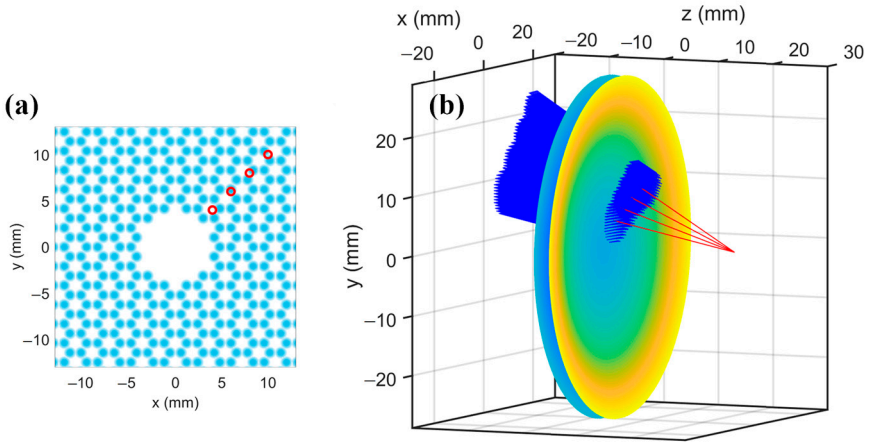

Figure 3. The three-dimensional ray tracing of the lens–eye system. (**a**) The selected positions of the chief rays on the lens surface for the determination of the gaze directions are represented by the red circles, whose coordinates are (4, 4), (6, 6), (8, 8), and (10, 10). (**b**) High-density ray tracing from an object point to the image space within a working aperture of 8 mm for each selected gaze direction. The red lines represent the light path of the chief rays.

The emergent wavefront at the vertex sphere was calculated by comparing the optical path length of each ray to that of the chief ray within the required aperture. Fourier transform of the generalized pupil function built on the calculated emergent wavefront within a pupil aperture of 6 mm in diameter was performed to obtain the point spread function (PSF) that represents the Fresnel diffraction pattern. The detection plane of PSF was set at the focus of the equivalent spherical power of the emergent wavefront, which refers to the focus of spectacle lenses without micro-structures.

The lenslet with +3.00 D addition power and the lenslet with −3.00 D addition power generate the opposite local phase delay, which, by design, create localized wavefront errors in the emergent wavefront, as shown in Figure 4. In both cases, the array-patterned phase delay caused by the lenslet array gives rise to the ultra-high RMS wavefront aberrations that force the intensity distribution of PSF to be spread significantly. As a result, the simulated images of an extended object by convolving the PSFs with the object are obviously blurred. Although both the addition power and the induced phase delay of the lenslet are opposite between PLARI and NLARI, there is a remarkable resemblance in the performance of PSF, image simulation, and modulation transfer function (MTF), as shown in Figure 5. Therefore, both PLARI and NLARI spectacle lenses provide the same image quality or equivalent image blur for the lens wearers.

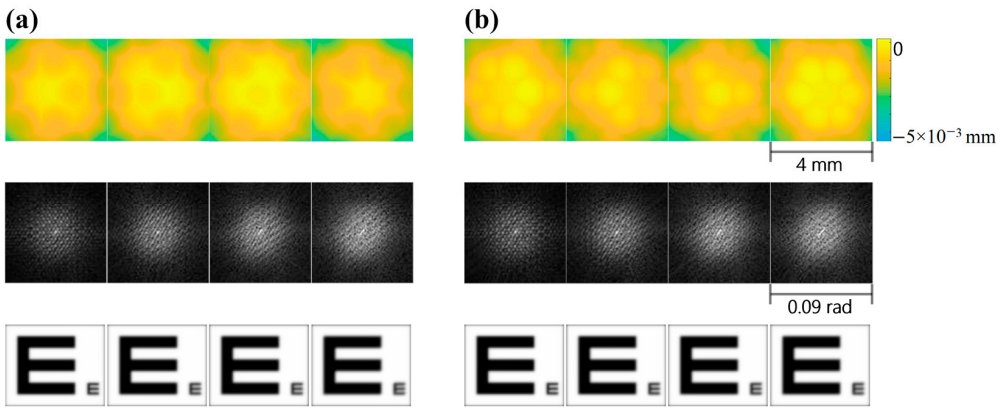

Figure 4. Imaging quality evaluation of (**a**) PLARI and (**b**) NLARI for increasing gaze angles, which are 13.3°, 19.5°, 25.2°, and 30.5° (from left to right). First row: Emergent wavefront. Second row: Point spread function (PSF). Third row: Simulated image of letter E.

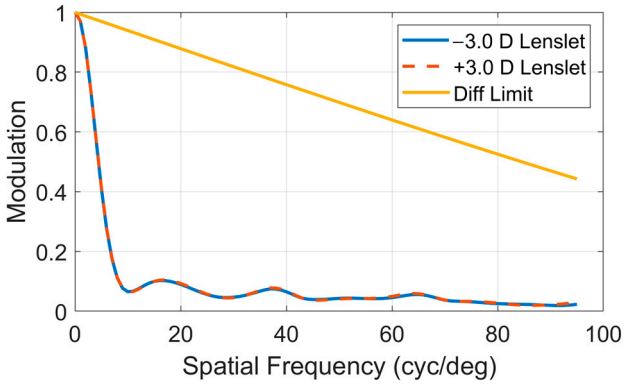

Figure 5. Calculated average MTF in whole circumference direction of LARI spectacle lens for gaze direction featured by chief ray position of (6, 6) on lens surface, as defined in Figure 3, with gaze angle of 19.5°.

3. Design of HOPE Spectacle Lens

Each lenslet working in the LARI spectacle lens can be considered as a phase element that provides additional low-order phase delay, which can form low-order wavefront aberration. Therefore, the array pattern of lenslets generates the spatial phase modulation to the wavefront, leading to the increase in RMS wavefront aberrations within the pupil aperture. A similar phase modulation effect can be achieved by using an array pattern of a high-order phase element (HOPE) that can generate high-order phase delay, which can form high-order wavefront. The advantage of using HOPEs instead of lenslet is the countless surface designs and surface description methods for the phase elements, which can provide numerous HOPE spectacle lens designs with a similar optical performance to the LARI spectacle lens.

Here, for example, Zernike polynomials are used to describe the surface of each HOPE within a circular aperture. Then, the aperture is cut into the shape of the inscribed regular hexagon. Each HOPE neighbored by six adjacent HOPEs, the HOPEs are arranged by a hexagonal array pattern and a fill factor of 100% to give rise to the micro-structures on the front lens surface. The micro-structures are absent in the central optical zone with a hexagonal aperture of about 8 mm in diameter. The surface of each HOPE can be described by high-order Zernick polynomials, such as trefoil, quadrafoil, pentafoil, and the mixed surfaces. For example, as shown in Figure 6, the surface of the O-HOPE design is described as $S_1(x, y) = \left|c_5^3 Z_5^3\right|$, $c_5^3 = 0.35$ μm, where Z_5^3 and c_5^3 stand for Zernike polynomial and coefficient of the 2nd trefoil. The surface of the T-HOPE design is described as $S_2(x, y) = \left|c_3^1 Z_3^1\right| + \left|c_3^{-1} Z_3^{-1}\right|$, $c_3^1 = c_3^{-1} = 0.25$ μm, where Z_3^1 and Z_3^{-1} stand for Zernike polynomial of the 2nd horizontal coma and 2nd vertical coma. Both of the HOPEs are arranged at a constant grid pitch of 1.32 mm. The base optic of the lens is the same as that used in the LARI spectacle lens.

The model of the HOPE spectacle lens was imported to the lens–eye system depicted in Figure 3 for imaging quality evaluation. As shown in Figure 7, the array-patterned HOPEs lead to the complicated spatial phase modulation of the emergent wavefront by the induced periodic high-order phase delay. As a result, the intensity distributions of PSFs are more diffused than in the case of the LARI spectacle lens. So, the blurred simulated images are obtained as expected. O-HOPE and T-HOPE spectacle lenses seem to have similar performance in image quality, as indicated by their calculated MTFs shown in Figure 8.

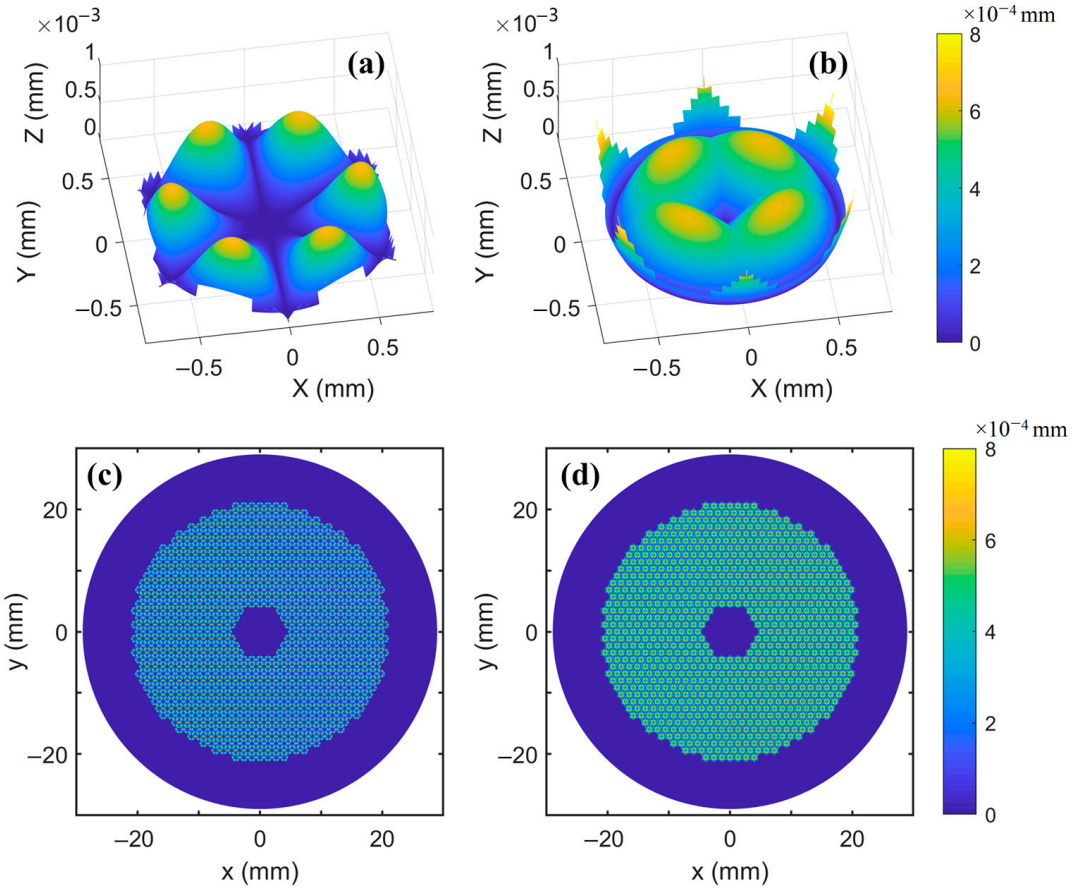

Figure 6. Micro-structure design of high-order phase elements (HOPEs) spectacle lens. Sag profiles of (**a**) O-HOPE and (**b**) T-HOPE are represented by Zernike polynomials. Hexagonal arrangement of (**c**) O-HOPE and (**d**) T-HOPE forms array-patterned micro-structures to be loaded on front lens surface.

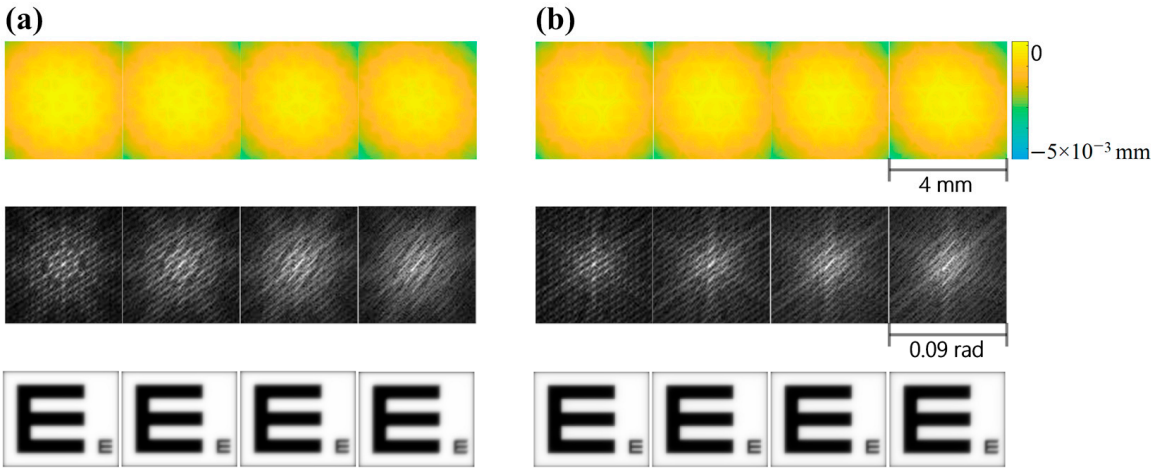

Figure 7. Imaging quality evaluation of (**a**) O-HOPE spectacle lens and (**b**) T-HOPE spectacle lens for increasing gaze angles, which are 13.3°, 19.5°, 25.2°, and 30.5° (from left to right). First row: Emergent wavefront. Second row: PSF. Third row: Simulated image of letter E.

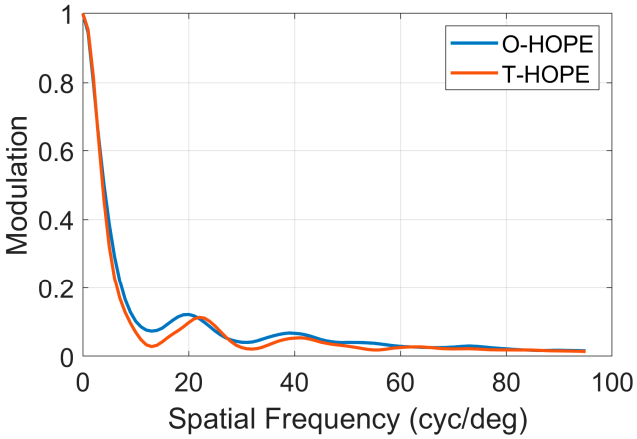

Figure 8. The calculated average MTF in the whole circumference direction of HOPE spectacle lens for the gaze direction featured by the chief ray position of (6, 6) on the lens surface, as defined in Figure 3, with a gaze angle of 19.5°.

4. Manufacture and Performance

For the high-precision manufacturing of these spectacle lenses, the sag profile of the lens front surface with micro-structures was first represented by a high-density point cloud based on a polar mesh within an aperture of 78 mm in diameter. The grid point elements are equally spaced along the radial direction with an incremental size of 10 μm and are circumferentially spaced with a fixed angular increment of 0.075°. Then, the spiral tool path required by the surface machining was generated by interpolation of the point cloud with the consideration of tool nose radius compensation. The diamond turning of the nickel-plated steel mold insert was performed by following the calculated tool path on a high-precision, numerically controlled lathe (Moore Nanotech 250UPL, LLC 230 Old Homestead Hwy, Swanzey, NH, USA). The finishing cutting with a depth of 4 μm provided the high-quality surface, as shown in Figure 9. These mold inserts were installed in a mold base that was loaded into an electric injection molding machine (FANUC ROBOSHOT Models, α-S150iA, Echternach, Luxembourg) for the mass production of the spectacle lenses using polycarbonate as the material. Under the illumination of a high-brightness light source, each molded spectacle lens generated a unique intensity distribution corresponding to the honeycomb-like contour pattern of the micro-structures embedded in the lens.

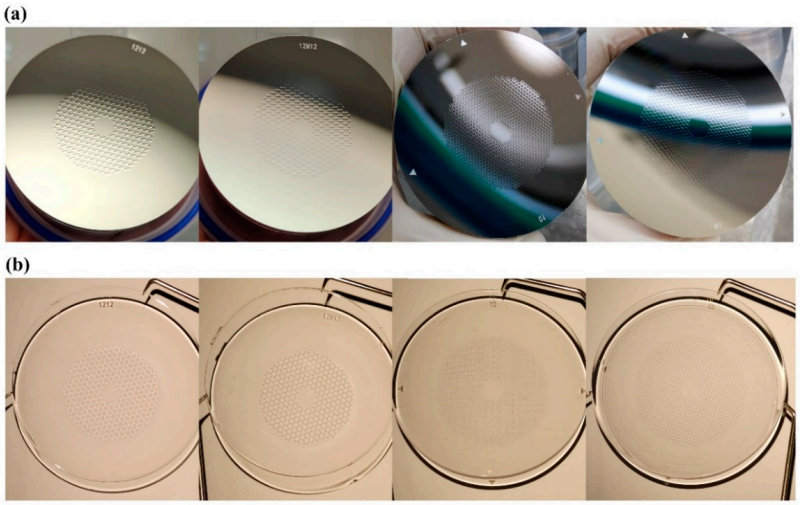

Figure 9. Injection molding of both LARI and HOPE spectacle lenses with aperture size of 75 mm in diameter. From left to right: PLARI, NLARI, O-HOPE, and T-HOPE. (**a**) Mold inserts manufactured by high-precision single-point diamond turning; (**b**) molded spectacle lenses under illumination.

To demonstrate the image characteristics likely experienced by the lens wearer, an imaging system that includes a display screen, spectacle lens, and mounted smartphone (X Fold, vivo) was constructed, as shown in Figure 10. The smartphone camera was aligned with the optical center of the spectacle lens, so the field of view (FOV) of the camera mimics the static FOV of lens wearer. The distance between the spectacle lens and the smartphone was set to be 55 mm, so the FOV of the camera can cover the whole aperture of the lens. As expected, image blur is observed for the FOV larger than 8°. The two kinds of LARI spectacle lenses produce similar results by comparing Figure 10b to Figure 10c. The images provided by the HOPE spectacle lenses are much more blurred as predicted by their lower value of MTF shown in Figure 8.

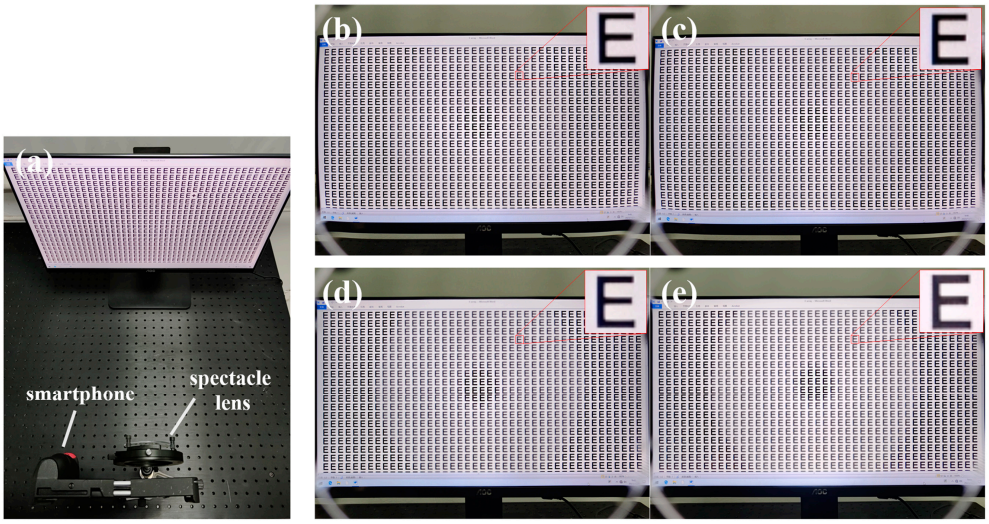

Figure 10. Images taken by smartphone camera through spectacle lens. (**a**) System configuration includes display screen, spectacle lens, and smartphone with mounting. (**b**) PLARI; (**c**) NLARI; (**d**) O-HOPE; (**e**) T-HOPE.

5. Discussion

The aim of this study was to propose a new possible mechanism of myopia control, which is image blur. At present, the spectacle lenses for myopia control are basically designed based on the lenslets of positive addition power, such as DIMS spectacle lens with lenslets of +3.5 D power and 50% fill factor [18], and MiYOSMART spectacle lens with lenslets of +3.95 D mean power and 40% fill factor [17]. However, the fill factor of the lenslets in LARI spectacle lenses is improved to 66.7%, and MTF analysis reveals that the LARI spectacle lenses have flatter and lower imaging quality compared to the DIMS spectacle lenses with lenslets of low fill factor [18]. In this work, the PLARI and NLARI spectacle lenses were designed for comparative study, especially the spectacle lens designed with lenslets of negative addition power, which were boldly proposed for the study of myopia control efficacy. The results of the study found that PLARI and NLARI spectacle lenses with opposite lenslet powers have a remarkable resemblance in the performance of PSF, MTF, and image simulation. Therefore, both PLARI and NLARI spectacle lenses provide the same image quality or equivalent image blur for the lens wearers, which may be speculated to have similar myopia control efficacy. According to the first-year clinical results of LARI spectacle lenses [20], both PLARI and NLARI spectacle lenses showed significantly slower myopia progression, breaking through the original myopia progression control theory based on myopic peripheral defocus on the retina, and possibly inferring the principle of image blur to explain the myopia control efficacy.

In addition, traditional spectacle lenses with lenslets are designed based on lenslets with positive addition power, and each lenslet provides the low-order phase delay, thus obtaining multipoint myopia defocus on the retina [12,18]. In order to further analyze the mechanism of myopia control, HOPE spectacle lenses were proposed and designed. The results show that O-HOPE and T-HOPE spectacle lenses seem to have similar performance in PSF, MTF, and image simulation, leading to the similar image quality for lens wearers. The HOPE spectacle lenses provide more blurred images compared to LARI spectacle lenses. The main advantage of the HOPE spectacle lenses is that there are countless choices of phase element, such as trefoil, quadrafoil, pentafoil, or the combination of several high-order terms. Without any low-order phase element, HOPE design can suppress the appearance of the defocus factor and maintain the effect of high-order phase modulation on the wavefront. The clinical trials of HOPE spectacle lenses for myopia control are currently ongoing.

Due to the large number of parameters for spectacle lens design, the comparative study of different parameters such as pupil size, central optical zone size of spectacle lens, and array-pattern of phase elements brings new challenges to clinical and theoretical research, which may affect the understanding of the working principles of the spectacle lens. The mechanism of myopia control has yet to be determined and needs further investigation.

6. Conclusions

In the scope of this work, the LARI micro-structure was developed and tailored to the new application in spectacle lens for myopia control via image blur. The simulation study demonstrates that the imaging characteristics are undistinguishable between the PLARI and NLARI spectacle lenses. It provides the opportunity to challenge the traditional ideal about myopia progression control via relatively myopic periphery defocus, if the ongoing RCT of both LARI spectacle lenses provides similar myopia control efficacy. Inspired by the direct relation between image blur and the RMS wavefront aberrations generated by the phase modulation of lenslet array in the LARI case, we expanded the design space of micro-structures to the HOPEs that can be described by Zernike polynomials and integrated on the lens surfaces. We validate the applicability of the proposed array-patterned micro-structure designs by injection molding the high-quality spectacle lenses with the help of ultra-precision fabrication of the micro-structures on the mold surface.

Author Contributions: Conceptualization, H.J. and Y.L. (Yiyu Li); methodology, H.J. and Y.L. (Yiyu Li); software, Z.Z., Q.Y. and Y.L. (Yiyu Li); validation, H.J., K.M. and Y.F.; formal analysis, H.J., Z.Z. and J.C.; investigation, Z.Z. and Y.L. (Yiqian Li); resources, K.M. and J.J.; data curation, Q.Y.; writing—original draft preparation, H.J.; writing—review and editing, Y.L. (Yiyu Li); visualization, Q.Y. and Y.L. (Yiqian Li); supervision, Y.L. (Yiyu Li); project administration, Y.L. (Yiyu Li) and H.J.; funding acquisition, Y.L (Yiyu Li). All authors have read and agreed to the published version of the manuscript.

Funding: This research received no external funding.

Institutional Review Board Statement: Not applicable.

Informed Consent Statement: Not applicable.

Data Availability Statement: The original contributions presented in the study are included in the article material; further inquiries can be directed to the corresponding author.

Acknowledgments: The authors wish to thank Xinquan Zhang and Yangqin Yu from Leading Optics for the valuable discussion about the diamond-turning process of the micro-structures, and would also like to thank Gino Optics for their support in the Rx lens fabrication.

Conflicts of Interest: The authors declare no conflicts of interest.

References

1. Lipson, M.J. The role of orthokeratology in myopia management. *Eye Contact Lens* **2022**, *48*, 189–193. [CrossRef]
2. Hiraoka, T. Myopia control with orthokeratology: A review. *Eye Contact Lens* **2022**, *48*, 100–104. [CrossRef] [PubMed]
3. Sankaridurg, P.; Donovan, L.; Varnas, S.; Ho, A.; Chen, X.A.; Martinez, A.; Fisher, S.; Lin, Z.; Smith, E.L.; Ge, J.A.; et al. Spectacle lenses designed to reduce progression of myopia: 12-month results. *Optom. Vis. Sci.* **2010**, *87*, 631–641. [CrossRef] [PubMed]
4. Skidmore, K.V.; Tomiyama, E.S.; Rickert, M.E.; Richdale, K.; Kollbaum, P. Retrospective review of the effectiveness of orthokeratology versus soft peripheral defocus contact lenses for myopia management in an academic setting. *Ophthalmic Physiol. Opt.* **2023**, *43*, 534–543. [CrossRef] [PubMed]
5. Li, N.; Lin, W.P.; Liang, R.X.; Sun, Z.W.; Du, B.; Wei, R.H. Comparison of two different orthokeratology lenses and defocus incorporated soft contact (DISC) lens in controlling myopia progression. *Eye Vis.* **2023**, *10*, 43. [CrossRef] [PubMed]
6. Li, Q.; Fang, F.Z. Advances and challenges of soft contact lens design for myopia control. *Appl. Opt.* **2019**, *58*, 1639–1656. [CrossRef]
7. Ramasubramanian, V.; Logan, N.S.; Jones, S.; Meyer, D.; Jaskulski, M.; Rickert, M.; Chamberlain, P.; Arumugam, B.; Bradley, A.; Kollbaum, P.S. Myopia control dose delivered to treated eyes by a dual-focus myopia-control contact lens. *Optom. Vis. Sci.* **2023**, *100*, 376–387. [CrossRef]
8. Sankaridurg, P.; Bakaraju, R.C.; Naduvilath, T.; Chen, X.; Weng, R.; Tilia, D.; Xu, P.; Li, W.N.; Conrad, F.; Smith, E.L.; et al. Myopia control with novel central and peripheral plus contact lenses and extended depth of focus contact lenses: 2 year results from a randomised clinical trial. *Ophthalmic Physiol. Opt.* **2019**, *39*, 294–307. [CrossRef] [PubMed]
9. Benavente-Pérez, A.; Nour, A.; Troilo, D. Axial eye growth and refractive error development can be modified by exposing the peripheral retina to relative myopic or hyperopic defocus. *Investig. Ophthalmol. Vis. Sci.* **2014**, *55*, 6765–6773. [CrossRef] [PubMed]
10. Atchison, D.A.; Rosén, R. The possible role of peripheral refraction in development of myopia. *Optom. Vis. Sci.* **2016**, *93*, 1042–1044. [CrossRef] [PubMed]
11. Gifford, P.; Gifford, K.L. The future of myopia control contact lenses. *Optom. Vis. Sci.* **2016**, *93*, 336–343. [CrossRef] [PubMed]
12. Lam, C.S.Y.; Tang, W.C.; Tse, D.Y.Y.; Lee, R.P.K.; Chun, R.K.M.; Hasegawa, K.; Qi, H.; Hatanaka, T.; To, C.H. Defocus incorporated multiple segments (DIMS) spectacle lenses slow myopia progression: A 2-year randomised clinical trial. *Br. J. Ophthalmol.* **2020**, *104*, 363–368. [CrossRef]
13. Bao, J.H.; Yang, A.; Huang, Y.Y.; Li, X.; Pan, Y.G.; Ding, C.L.; Lim, E.W.; Zheng, J.W.; Spiegel, D.P.; Drobe, B.; et al. One-year myopia control efficacy of spectacle lenses with aspherical lenslets. *Br. J. Ophthalmol.* **2022**, *106*, 1171–1176. [CrossRef] [PubMed]
14. Liu, X.T.; Wang, P.Q.; Xie, Z.; Sun, M.H.; Chen, M.F.; Wang, J.F.; Huang, J.; Chen, S.Y.; Chen, Z.H.; Wang, Y.L.; et al. One-year myopia control efficacy of cylindrical annular refractive element spectacle lenses. *Acta Ophthalmol.* **2023**, *101*, 651–657. [CrossRef] [PubMed]
15. Radhakrishnan, H.; Lam, C.S.Y.; Charman, W.N. Multiple segment spectacle lenses for myopia control. Part 2: Impact on myopia progression. *Ophthalmic Physiol. Opt.* **2023**, *43*, 1137–1144. [CrossRef]
16. Papadogiannis, P.; Börjeson, C.; Lundström, L. Comparison of optical myopia control interventions: Effect on peripheral image quality and vision. *Biomed. Opt. Express* **2023**, *14*, 3125–3137. [CrossRef] [PubMed]
17. Gantes-Nuñez, J.; Jaskulski, M.; López-Gil, N.; Kollbaum, P.S. Optical characterisation of two novel myopia control spectacle lenses. *Ophthalmic Physiol. Opt.* **2023**, *43*, 388–401. [CrossRef] [PubMed]
18. Jaskulski, M.; Singh, N.K.; Bradley, A.; Kollbaum, P.S. Optical and imaging properties of a novel multi-segment spectacle lens designed to slow myopia progression. *Ophthalmic Physiol. Opt.* **2020**, *40*, 549–556. [CrossRef] [PubMed]
19. Wolffsohn, J.S.; Hill, J.S.; Hunt, C.; Young, G. Visual impact of diffusion optic technology lenses for myopia control. *Ophthalmic Physiol. Opt.* **2024**, *44*, 1398–1406. [CrossRef]
20. Su, B.; Cho, P.; Vincent, S.J.; Zheng, J.; Chen, J.; Ye, C.; Wang, T.; Zhang, J.; Zhang, K.; Lu, F.; et al. Novel lenslet-array-integrated spectacle lenses for myopia control: A 1-year randomized, double-masked, controlled trial. *Ophthalmology* **2024**, *131*, 1389–1397. [CrossRef] [PubMed]
21. Li, Y.Y.; Zhao, Z.W.; Yuan, Q.; Li, Y.X.; Ma, K.; Fu, Y.Y.; Chen, J.J.; Jiang, J. Array-Patterned Micro-Structures in Spectacle Lens for Myopia Control via Image Blurry. In Proceedings of the SPIE Photonics Asia 2024, Nantong, China, 13 October 2024; pp. 13237–13240.
22. Xia, R.; Fu, Y.; Ma, K.; Chen, S.; Pan, J.; Zhou, C.; Feng, H.; Qu, J.; Li, Y. Surface astigmatism correction using segmented freeform surfaces for a progressive addition lens. *Opt. Express* **2022**, *30*, 43384–43397. [CrossRef]